

# Lawrence Berkeley National Laboratory

## LBL Publications

### Title

Revealing the role of electron-electron correlations by mapping dissociation of highly excited D<sub>2</sub><sup>+</sup> using ultrashort XUV pulses

### Permalink

<https://escholarship.org/uc/item/3zb2g9hj>

### Journal

Physical Review A, 97(6)

### ISSN

2469-9926

### Authors

Martin, L

Bello, RY

Hogle, CW

et al.

### Publication Date

2018-06-01

### DOI

10.1103/physreva.97.062508

Peer reviewed

## Important Notice to Authors

**No further publication processing will occur until we receive your response to this proof.**

Attached is a PDF proof of your forthcoming article in PRA. Your article has 9 pages and the Accession Code is **XH10238A**.

Please note that as part of the production process, APS converts all articles, regardless of their original source, into standardized XML that in turn is used to create the PDF and online versions of the article as well as to populate third-party systems such as Portico, Crossref, and Web of Science. We share our authors' high expectations for the fidelity of the conversion into XML and for the accuracy and appearance of the final, formatted PDF. This process works exceptionally well for the vast majority of articles; however, please check carefully all key elements of your PDF proof, particularly any equations or tables.

Figures submitted electronically as separate files containing color appear in color in the online journal. However, all figures will appear as grayscale images in the print journal unless the color figure charges have been paid in advance, in accordance with our policy for color in print (<https://journals.aps.org/authors/color-figures-print>).

### Specific Questions and Comments to Address for This Paper

- 1 Please check our change here. Please refer to <https://journals.aps.org/authors/new-novel-policy-physical-review>
- 2 We have spelled out HHG at its only use. Please check.
- 3 Please ensure that the equation is set properly, especially regarding the number 1 and the letter l.
- 4 Please check our deletion here (the paper has no appendix). Please revise if there should be a citation to another part of the paper.
- 5 Please complete Ref. [3] (journal name is missing).
- 6 Please complete Ref. [4].
- 7 Please complete Ref. [7]
- 8 Ref. [10] has been updated. Please check.
- 9 Please complete Ref. [11].
- 10 Please complete Ref. [12].
- 11 Please complete Ref. [14].
- 12 Ref. [15]: Page number added. Please check.
- 13 Please complete Ref. [16].
- 14 Please complete Ref. [17].
- 15 Please complete Ref. [19].
- 16 Please complete Ref. [20].
- 17 Please complete Ref. [23].
- 18 Ref. [26]: Incorrect volume and page number removed, doi added. Please check.
- 19 Please complete Ref. [32].
- 20 Ref. [34]: Please replace 'more information' with a brief description for the reader of what can be found in the Supplemental Material.

Open Funder Registry: Information about an article's funding sources is now submitted to Crossref to help you comply with current or future funding agency mandates. Crossref's Open Funder Registry (<https://www.crossref.org/services/funder-registry/>) is the definitive registry of funding agencies. Please ensure that your acknowledgments include all sources of funding for your article following any requirements of your funding sources. Where possible, please include grant and award ids. Please carefully check the following funder information we have already extracted from your article and ensure its accuracy and completeness:

DOE Office of Basic Energy Sciences, DE-FG02-99ER14982

MINECO, FIS2013-42002-R

Vicerrectoría de Investigación, E01538

COLCIENCIAS, 111565842968

US Department of Energy, DE-AC02-05CH11231

### Other Items to Check

- Please note that the original manuscript has been converted to XML prior to the creation of the PDF proof, as described above. Please carefully check all key elements of the paper, particularly the equations and tabular data.
- Title: Please check; be mindful that the title may have been changed during the peer-review process.
- Author list: Please make sure all authors are presented, in the appropriate order, and that all names are spelled correctly.
- Please make sure you have inserted a byline footnote containing the email address for the corresponding author, if desired. Please note that this is not inserted automatically by this journal.
- Affiliations: Please check to be sure the institution names are spelled correctly and attributed to the appropriate author(s).
- Receipt date: Please confirm accuracy.

- **Acknowledgments:** Please be sure to appropriately acknowledge all funding sources.
- **Hyphenation:** Please note hyphens may have been inserted in word pairs that function as adjectives when they occur before a noun, as in “x-ray diffraction,” “4-mm-long gas cell,” and “ $R$ -matrix theory.” However, hyphens are deleted from word pairs when they are not used as adjectives before nouns, as in “emission by x rays,” “was 4 mm in length,” and “the  $R$  matrix is tested.”

Note also that Physical Review follows U.S. English guidelines in that hyphens are not used after prefixes or before suffixes: superresolution, quasiequilibrium, nanoprecipitates, resonancelike, clockwise.

- Please check that your figures are accurate and sized properly. Make sure all labeling is sufficiently legible. Figure quality in this proof is representative of the quality to be used in the online journal. To achieve manageable file size for online delivery, some compression and downsampling of figures may have occurred. Fine details may have become somewhat fuzzy, especially in color figures. The print journal uses files of higher resolution and therefore details may be sharper in print. Figures to be published in color online will appear in color on these proofs if viewed on a color monitor or printed on a color printer.
- Please check to ensure that reference titles are given as appropriate.
- Overall, please proofread the entire *formatted* article very carefully. The redlined PDF should be used as a guide to see changes that were made during copyediting. However, note that some changes to math and/or layout may not be indicated.

### Ways to Respond

- **Web:** If you accessed this proof online, follow the instructions on the web page to submit corrections.
- **Email:** Send corrections to [praproofs@aptaracorp.com](mailto:praproofs@aptaracorp.com)  
Subject: **XH10238A** proof corrections
- **Fax:** Return this proof with corrections to +1.703.791.1217. Write **Attention:** PRA Project Manager and the Article ID, **XH10238A**, on the proof copy unless it is already printed on your proof printout.

## Revealing the role of electron-electron correlations by mapping dissociation of highly excited $D_2^+$ using ultrashort XUV pulses

L. Martin,<sup>1</sup> R. Y. Bello,<sup>2</sup> C. W. Hogle,<sup>1</sup> A. Palacios,<sup>2</sup> X. M. Tong,<sup>3</sup> J. L. Sanz-Vicario,<sup>4</sup> T. Jahnke,<sup>5</sup> M. Schöffler,<sup>5</sup> R. Dörner,<sup>5</sup> Th. Weber,<sup>6</sup> F. Martín,<sup>2,7,8</sup> H. C. Kapteyn,<sup>1</sup> M. M. Murnane,<sup>1</sup> and P. Ranitovic<sup>1,6,9</sup>

<sup>1</sup>*JILA and Department of Physics, University of Colorado and NIST, Boulder, Colorado 80309, USA*

<sup>2</sup>*Departamento de Química, Universidad Autónoma de Madrid, Cantoblanco, 28049 Madrid, Spain*

<sup>3</sup>*Center for Computational Sciences, University of Tsukuba, Ibaraki 305-8573, Japan*

<sup>4</sup>*Grupo de Física Atómica y Molecular, Instituto de Física, Universidad de Antioquía, Medellín, Colombia*

<sup>5</sup>*Institut für Kernphysik, University Frankfurt, Max von Laue Strasse 1, D-60438 Frankfurt, Germany*

<sup>6</sup>*Lawrence Berkeley National Laboratory, 1 Cyclotron Road, Berkeley, California 94720, USA*

<sup>7</sup>*Instituto Madrileño de Estudios Avanzados en Nanociencia (IMDEA Nano), Campus de Cantoblanco, 28049 Madrid, Spain*

<sup>8</sup>*Condensed Matter Physics Center (IFIMAC), Universidad Autónoma de Madrid, 28049 Madrid, Spain*

<sup>9</sup>*Laboratorium für Physikalische Chemie, ETH Zürich, 8093 Zürich, Switzerland*



(Received 3 August 2017; published xxxxxx)

Understanding electron-electron correlations in matter ranging from atoms to solids represents a grand challenge for both experiment and theory. These correlations occur on attosecond timescales and have only recently become experimentally accessible. In the case of highly excited systems, the task of understanding and probing correlated interactions is even greater. In this work, we combine state-of-the-art light sources and advanced detection techniques with *ab initio* calculations to unravel the role of electron-electron correlation in  $D_2$  photoionization by mapping the dissociation of a highly excited  $D_2^+$  molecule. Correlations between the two electrons dictate the pathways along which the molecule dissociates and lead to a superposition of excited ionic states. Using 3D Coulomb explosion imaging and electron-ion coincidence techniques, we assess the relative contribution of competing parent ion states to the dissociation process for different orientations of the molecule with respect to the laser polarization, which is consistent with a shake-up ionization process. As a step toward observing coherent superposition experimentally, we map the relevant nuclear potentials using Coulomb explosion imaging and show theoretically that such an experiment could confirm this coherence via two-path interference.

DOI: [10.1103/PhysRevA.00.002500](https://doi.org/10.1103/PhysRevA.00.002500)

### I. INTRODUCTION

As the simplest and most abundant molecule in the universe, the hydrogen molecule represents an important test bed for developing a complete understanding of molecular physics on the smallest spatial and fastest vibrational temporal scales. For example, electron double-slit experiments have been performed on the level of a single molecule [1], fast nuclear motions have been observed [2,3], and tests of quantum electrodynamic concepts have been implemented in chemical systems [4]. Ultrafast laser technology and ultrafast high-harmonic pulses enable unprecedented capabilities for capturing and controlling electron dynamics in small atoms, molecules, and materials on femtosecond and even subfemtosecond timescales [5–18]. In parallel with the rapid development of novel ultrafast experimental techniques, full quantum simulations that include correlated electron-electron and electron-nuclear motions have become possible in simple diatomic molecules such as  $H_2$  and  $D_2$ .

In this context, extreme ultraviolet (XUV) high-harmonic pulses and infrared (IR) fields have been successfully used to control molecular dissociation of  $H_2/D_2$  after photoionization by steering the reaction with unprecedented precision [19–23]. More recently, coherent attosecond pulse trains in the vacuum UV regime made it possible to coherently control the dynamics

of an excited neutral  $D_2$  molecule for the first time [24]. Previously, the dynamics of high-lying electronic states of a hydrogen molecule was out of reach for traditional VUV sources typically used in femtochemistry. Novel applications have also used attosecond XUV techniques to unravel the photoionization delays between direct and the shake-up ionization in atomic targets [25] or to explore the effect of the coupled electron and nuclear motion in hydrogen molecules [26]. In the helium atom, it was found that due to the pure electron-electron correlation effects, the photoionization delays are occurring on a sub-10-attosecond timescale. Trying to progress from a two-electron helium atom to a simple two-electron molecular system and understanding electron-electron correlations in a highly excited hydrogen molecule are particularly challenging from both a theoretical and an experimental point of view. In particular, understanding electron-electron correlations and the coherences in a rapidly dissociating molecular system, where nearly exact theoretical calculations are still tractable, clearly helps us to develop concepts necessary to understand dynamics in more complex molecular systems or correlated materials.

In this work, we combine ultrafast and synchrotron XUV sources with electron-ion 3D coincidence imaging techniques to explore the relevance of electron-electron correlations in the dissociative photoionization of  $D_2$  leading to a highly excited  $D_2^{+*}$  molecule—the region whose dynamics has not been

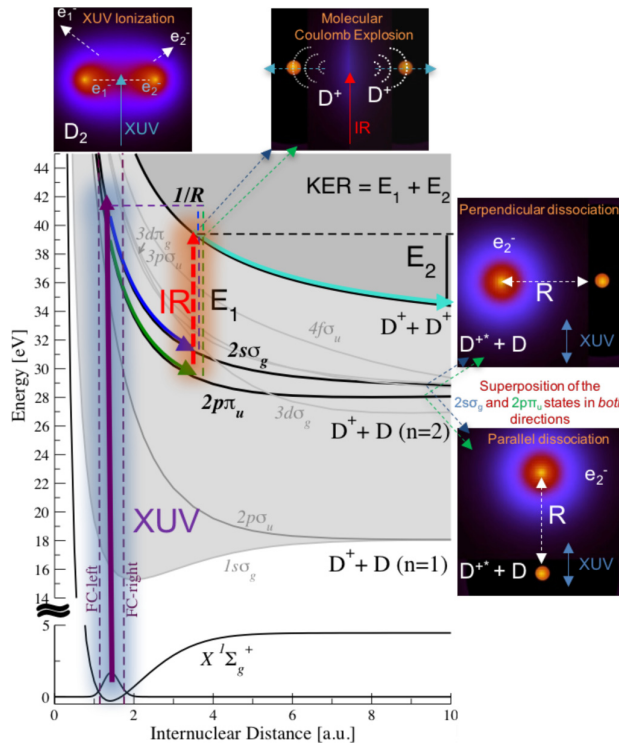


FIG. 1. Correlated electron-electron and nuclear wave packet dynamics in  $D_2 + h\nu \rightarrow D_2^+ + e^-$ . Ultrashort and synchrotron XUV pulses with energy centered at 42.6 eV (42 eV) were used to excite a highly correlated manifold of electronic states in  $D_2^+$ . The subsequent dissociative process, following the photoionization, was mapped by using time-resolved IR pulses and Coulomb-explosion imaging. Dashed vertical lines indicate the Franck-Condon boundaries.

79 explored thus far. In particular, we determine the branching  
 80 ratios for different dissociative ionization channels associated  
 81 with this molecular shake-up process as a function of the  
 82 molecular orientation with respect to the laser and XUV  
 83 polarization. As seen in Fig. 1, a short 42.6 eV high-harmonic  
 84 pulse first ionizes the neutral molecule, which is hereby excited  
 85 into high-lying dissociative electronic states of the parent  
 86 ion. Although most of the  $D_2^+$  molecules are left in the  
 87 ground state of the ion, a small fraction of them undergoes an  
 88 excitation-ionization (shake-up) step, where a second electron  
 89 is excited simultaneously during the photoionization process.  
 90 Such a process is depicted in the upper-left panel of Fig. 1, and  
 91 is only possible when the two electrons are tightly correlated  
 92 [27]. Due to the steep potentials of the highly excited  $H_2^+$   
 93 states, the outgoing electron can continuously share the energy  
 94 with the  $H_2^{+*}$  ion left behind. By using a time-delayed infrared  
 95 probe pulse, combined with electron-ion coincidence imaging  
 96 techniques, we map the energy distributions of the molecular  
 97 fragments, which provide an indirect measurement of the  
 98 nuclear potentials. When combined with advanced *ab initio*  
 99 calculations that include the coupled nuclear and electronic  
 100 motions, we draw two significant conclusions. First, we find  
 101 that the dynamics, captured in the molecular Coulomb explosion  
 102 (upper-right panel of Fig. 1), is dominated by the excitation  
 103 of the  $2s\sigma_g$  state, regardless of the molecular orientation with

104 respect to the light polarization. The experimental data rule  
 105 out the naïve model based on a single-active electron picture:  
 106 one-electron  $s \rightarrow p$  dipole transitions within an independent  
 107 particle model should favor excitation into the  $2p\pi_u$  state,  
 108 particularly for the perpendicular orientation. Second, the  
 109 dissociation process results in a superposition of nuclear  
 110 wave packets evolving simultaneously on different potential  
 111 energy curves of the parent ion, mainly those associated with  
 112 the  $2p\pi_u$  and  $2s\sigma_g$  electronic states. Since these states  
 113 dissociate into the same energy limit, Coulomb imaging of the  
 114 dissociation process always reflects a mixture of both states.  
 115 Simulations confirm the presence of coherence and suggest  
 116 that a similar Coulomb imaging experiment could readily  
 117 observe it by measuring interference between the  $2p\pi_u$  and  
 118  $2s\sigma_g$  states. Moreover, by using the synchrotron XUV photons  
 119 of similar energy, we obtain molecular-frame photoelectron  
 120 angular distributions (MFPADs) showing strong electron-  
 121 electron correlation effects. In this way, we capture effects that  
 122 help us fully understand how electron interactions drive the  
 123 nuclear dynamics in the excitation process of the molecular  
 124 ion Rydberg states. We offer this time-resolved study of the  
 125 coupled electron-nuclear dynamics and quantitative analysis  
 126 of the electron-electron correlation effects that govern the  
 127 branching ratios for different orientations of the  $D_2^{+*}$  molecule  
 128 dissociating into the  $n = 2$  limit.

## 129 II. POLARIZATION ORIENTATION EFFECTS IN THE 130 TIME-RESOLVED ELECTRON-NUCLEAR DYNAMICS

131 We use a 42.6 eV XUV ultrashort pump pulse, synchronized  
 132 with a probe IR laser (784 nm) to, first, excite and then  
 133 map the dynamics of the highly excited molecular ion in a  
 134 COLTRIMS (cold target recoil ion momentum spectroscopy)  
 135 geometry [28]. The absorption of the XUV pulse ionizes the  
 136 neutral  $D_2$  molecule, creating a superposition of highly excited  
 137 electronic states in the molecular ion, as shown in Fig. 1.  
 138 The excited  $D_2^{+*}$  ion can then dissociate along several co-  
 139 herently populated pathways, upon the XUV photoionization,  
 140 leading to  $D^+ + D(n = 1)$  [corresponding to the  $D_2^+(1s\sigma_g$  and  
 141  $2p\sigma_u)$  molecular states] and  $D^+ + D(n = 2)$  [corresponding  
 142 to  $D_2^+(2s\sigma_g, 3p\sigma_u, 3d\sigma_g, 2p\pi_u, 3d\pi_g, 4f\sigma_u)$ ]. Here  $n$  is the  
 143 principle quantum number. As the molecular ion dissociates,  
 144 with the nuclei following the steep potential energy curves  
 145 of the  $D_2^{+*}$  states, the fragmentation dynamics is mapped  
 146 by ejecting the second electron using a strong IR laser field.  
 147 The delayed arrival of the IR pulse interrupts the dissociation  
 148 process  $D_2^{+*} \rightarrow D^+ + D(n)$  at a specific time, by ejecting the  
 149 second electron and leaving behind two bare deuterons that  
 150 undergo Coulomb explosion. The latter step is equivalent to  
 151 projecting the superposition of nuclear wave packets, created  
 152 by the XUV pulse, onto the Coulombic  $1/R$  potential energy  
 153 curve associated with the doubly ionized molecule (where  $R$  is  
 154 the internuclear separation). The kinetic energy release (KER)  
 155 and emission direction (parallel or perpendicular to the laser  
 156 polarization) of the two Coulomb-exploding deuterons is then  
 157 measured as a function of the XUV-IR time delay.

158 For the experimental pump-probe setup, we have used a  
 159 high-power (25 W), high repetition rate (10 kHz) Ti:sapphire  
 160 laser system coupled to a COLTRIMS coincidence electron-  
 161 ion detection setup. Most of the laser energy ( $\approx 1.7$  mJ) was

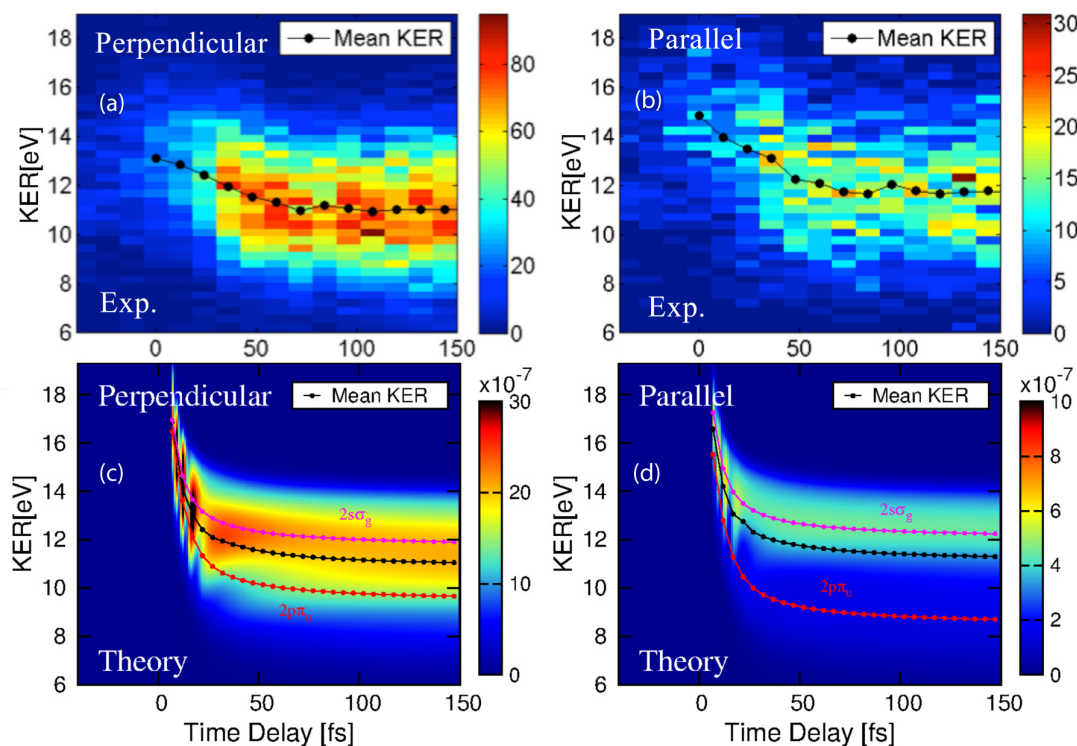


FIG. 2. Measured and calculated dissociative pathways of the highly excited  $D_2^+$  electronic states. (a) and (b) Measured nuclear kinetic energy release (NKE or KER) versus IR time delay for the dissociation events perpendicular and parallel to the XUV/IR polarization direction. The dotted line represents the mean KER of the ion yield for each IR delay value. In the perpendicular case, the coherent superposition of the  $2s\sigma_g$  and  $2p\pi_u$  dissociative pathways gives a slightly lower mean KER curve compared with the parallel case, where the  $2s\sigma_g$  is the largest contribution. (c) and (d) Theoretical calculations for the NKE vs IR time delay with two dissociative pathways, taking into account electron-electron correlation and coupled nuclear wave packet dynamics, for the parallel and perpendicular orientation of the molecule with respect to the light polarization. In (c) and (d) we also include the mean KER corresponding to two truncated simulations where only one individual (incoherent) path is included:  $2p\pi_u$  in red dotted line or  $2s\sigma_g$  in magenta dotted line.

162 coupled into a waveguide filled with Ar to generate harmonics,  
 163 which were then refocused into a supersonic  $D_2$  gas target  
 164 using a pair of XUV multilayer mirrors, coated to reflect the  
 165 harmonic centered at 42.6 eV, as shown in Fig. 1. The central  
 166 photon energies of the harmonics were controlled by tuning  
 167 the gas pressure in the waveguide, while COLTRIMS enables  
 168 simultaneous detection of ion and electron 3D momenta [29–  
 169 31], allowing us to analyze both single and double ionization  
 170 events in coincidence with electrons, and differentiate various  
 171 ionization channels. We infer initial molecular orientation  
 172 relative to the laser polarization from the orientation of the  
 173 molecular fragments. The residual laser energy was spatially  
 174 and temporally recombined with the high harmonic beam in  
 175 a collinear geometry. By using a delay stage with a 10 cm  
 176 range and a 260 as step size, we could scan from attosecond  
 177 to femtosecond relative time delays. The duration of the high-  
 178 harmonic-generation pulse was  $\approx 10$  fs, while the IR pulse  
 179 duration was 30 fs. The probe IR intensity was  $5 \times 10^{12}$  W/cm<sup>2</sup>.  
 180 The IR intensity is strong enough to ionize the excited states of  
 181  $D_2^{+*}$ , while it is too weak to excite or ionize the ground state of  
 182  $D_2$ . The electron-ion coincidence experiments were performed  
 183 at beamline 9.3.2 of the Advanced Light Source synchrotron  
 184 ring at the Lawrence Berkeley National Laboratory applying  
 185 the COLTRIMS technique as well. The 3D-vector momenta

186 of the electrons and ions were calculated from the position  
 187 of impact and the times of flight of each particle; from the  
 188 momenta the directions and kinetic energies were derived and  
 189 transformed into the molecular frame. Because of the light  
 190 electron mass, the electron momentum is about 2.5% of the  
 191 heavy-particle momentum only, leading to a nearly back-to-  
 192 back fragmentation of the  $D^+$  ion and D atom, which hence  
 193 represents the molecular axis at the time of photodissociation.

194 The measured time-resolved double-ionization yields,  
 195 which map how the excited molecule dissociates along several  
 196 potential energy curves, are shown in Fig 2. In Figs. 2(a) and  
 197 2(b), we show the experimental KER distribution of the two  $D^+$   
 198 ions (originating from the same  $D_2^{+*}$  molecule), as a function  
 199 of the delay between the XUV pump and the IR probe pulses,  
 200 for the molecules dissociating perpendicular and parallel to  
 201 the XUV polarization, respectively. In Figs. 2(c) and 2(d) we  
 202 present the corresponding calculated KERs. The simulation  
 203 takes into account *both* electron-electron correlation during  
 204 the ionization process and the coupled nuclear wave packet  
 205 dynamics during the dissociation. The agreement between  
 206 experiment and theory depicting the branching ratios of the  
 207  $2p\pi_u$  and  $2s\sigma_g$  states is very good. Additionally, the theory  
 208 shows quantum beating modes for short time delays. Those  
 209 are associated with transitions via the  $2p\pi_u$  and  $2s\sigma_g$  ionic

states that reflect as oscillations in the double-ionization yields for delays of 20–30 fs [see Figs. 2(c) and 2(d)]. For the theoretical simulations, we used an *ab initio* method to describe the interaction with the attosecond XUV pulse. The ionization probabilities for the one-photon absorption process from the ground state of the  $D_2$  molecule are obtained from the exact solution of the time-dependent Schrödinger equation including electron correlation terms and nuclear motion. In brief, the time-dependent wave function is expanded in a basis set of Born-Oppenheimer states, resulting from an  $L^2$  close coupling method. In this expansion, the bound states of  $D_2$  are obtained by performing a configuration interaction calculation in a basis of antisymmetrized products of one-electron functions, and the continuum states are obtained by solving the multichannel scattering equations in a basis of uncoupled continuum states that are written as products of a one-electron wave function for the bound electron and an expansion on spherical harmonics and  $B$ -spline functions for the continuum electron. The multichannel expansion includes the six lowest ionic states ( $1s\sigma_g, 2p\sigma_u, 2p\pi_u, 2s\sigma_g, 3d\sigma_g$ , and  $3p\sigma_u$ ) and partial waves for the emitted electron up to a maximum angular momentum  $l_{\max} = 7$  enclosed in a box of 60 a.u., which amounts up to around 61 000 discretized continuum states. We thus compute the photoionization amplitudes for linearly polarized light for the process  $D_2(^1\Sigma_g^+) + h\nu \rightarrow [D_2^+(n\lambda_{g,u}) + e_1^-(l)]^1\Lambda_u$ , where  $^1\Lambda_u$  corresponds to the total final symmetry ( $^1\Sigma_u^+$  for parallel transitions and  $^1\Pi_u$  for perpendicular ones). For a given final symmetry, for instance  $^1\Pi_u$ , electrons will be ejected with even angular momenta leaving behind the ion in the  $D_2^+(2p\pi_u)$  state and odd angular momenta leaving behind the  $D_2^+(2s\sigma_g)$  state. We have found that the excitation probability for populating doubly excited  $Q_3$  and  $Q_4$  states, which lie in the vicinity of the above  $D_2^+$  states and autoionize on a femtosecond timescale, was significantly smaller than the probability for ionization + excitation into the states that correlate to the  $n = 2$  limit. Thus, the contribution to the total double-ionization yield from these states, in this experiment, is negligible. We have checked that for the electron kinetic energies involved in the single-ionization process considered in this work, the transition amplitudes are converged. We computed the one-photon ionization probabilities after the interaction with a 7 fs duration XUV pulse centered at 42.6 eV (42 eV to compare with the synchrotron radiation simulations) and with an intensity of  $10^{12}$  W/cm<sup>2</sup>. Then, the wave packet created in the highly excited ion after interaction with the pump XUV pulse can be written as a coherent sum over vibronic states associated with the  $D_2^{+*}$  ionic channels  $\alpha = 2s\sigma_g, 3p\sigma_u, 3d\sigma_g, 2p\pi_u, 3d\pi_g, 4f\sigma_u$ , and an electron in the continuum with energy  $\varepsilon_\alpha$ :

$$\Psi(E, t) = \sum_{\alpha} \sum_{\varepsilon_{\alpha}} \sum_{\nu_{\alpha}} C_{\alpha, \varepsilon_{\alpha}, \nu_{\alpha}} e^{-iE_{\varepsilon_{\alpha}, \nu_{\alpha}} t} \psi_{\alpha, \varepsilon_{\alpha}}(\mathbf{r}, \mathbf{R}) \chi_{\nu_{\alpha}}(R). \quad (1)$$

In this expression, the vibronic states with energies  $E_{\varepsilon_{\alpha}, \nu_{\alpha}}$  are described as a product of an electronic ( $\psi_{\alpha, \varepsilon_{\alpha}}$ ) and a nuclear ( $\chi_{\nu_{\alpha}}$ ) wave function, corresponding respectively to the electronic ( $\varepsilon_{\alpha}$ ) and vibrational ( $\nu_{\alpha}$ ) continua associated with the  $\alpha$  channel. The coefficients  $C_{\alpha, \varepsilon_{\alpha}, \nu_{\alpha}}$  are the accurately computed single-ionization amplitudes. Notice that, for each

channel  $\alpha$ , the total energy  $E$  is shared by both electrons and nuclei. When this wave packet is interrogated by the probe pulse, leading to an emission of the second electron and subsequent Coulomb explosion, different paths leading to the same KER are possible. The action of the delayed IR field to induce the full breakup of the molecule is modeled as a sudden vertical transition in which the  $D_2^+$  nuclear wave packet is projected onto the  $1/R$  potential energy curve of the doubly ionized molecule, using the FC approximation; therefore the KER differential double ionization probability is given by

$$P(\text{KER}, t) \propto \sum_{\varepsilon_{\alpha}} \left| \sum_{\alpha} \sum_{\nu_{\alpha}} \langle \chi_{\nu_{\alpha}} | \chi_{\nu_{\alpha}} \rangle e^{-iE_{\varepsilon_{\alpha}, \nu_{\alpha}} t} C_{\alpha, \varepsilon_{\alpha}, \nu_{\alpha}} \right|^2. \quad (2)$$

This equation is the result of the following assumptions for the probing step: (i) all electronic dipole couplings between the vibronic states populated by the pump pulse and those populated by the IR pulse are independent of the internuclear distance, and (ii) the energy of the electron emitted by the pump pulse is preserved during the probing step. Both are reasonable approximations for the structureless double electronic continuum that is reached by the combination of the pump and the probe pulses. Equation (2) reveals the relative phases between the vibronic states that conform to the wave packet in (1), giving rise to the observed oscillations in  $P(\text{KER}, t)$  as a function of  $t$ . As all of the  $\alpha$  channels contained in the pumped wave packet dissociate into the same limit,  $H(n=2) + H^+$ , the amplitude of the oscillations eventually vanishes for longer time delays ( $R$ ). The oscillations are not seen in the experimental data mostly because the ionization by the IR probe pulse requires absorption of many photons, a process that connects several dipole matrix elements, and not a simple projection of the  $D_2^+$  wave packet into the  $1/R$  state.

To better see the individual contributions of the wave packets associated with the highly excited ion, in Fig. 3 we plot the KER distributions, i.e., vertical cuts from Fig. 2, for the perpendicular and parallel orientations corresponding to two chosen time delays: 24 fs in the upper panels and 60 fs in the lower panels. We observe a very good agreement between the experimental and theoretical results, with distinct time-dependent KER profiles for different molecular orientation. Note that irrespective of the orientation of the molecule relative to the polarization and the time delay between the two photon pulses, the maximum of the KER distribution does not coincide with the maxima of the individual channels  $2p\pi_u$  or  $2s\sigma_g$  (yellow and violet full lines in Fig. 3, respectively), which in turn appear at different kinetic energies. On the contrary, the molecule tends to dissociate in a superposition of the  $2p\pi_u$  and  $2s\sigma_g$  states. For the dissociation in the direction perpendicular to the XUV polarization, the  $2s\sigma_g$  and the  $2p\pi_u$  states are equally contributing to the overall KER shape. On the other hand, the  $2s\sigma_g$  dominates the dissociation in the parallel direction [Fig. 3(b)]. The differences between the  $2p\pi_u$  and  $2s\sigma_g$  channels are a consequence of the energy and  $R$  dependence of the electronic dipole couplings. It is the relative value of these couplings that is at the origin of the actual profiles observed in the double-ionization yields (orange full line in Fig. 3). This graph suggests that the  $D^+$  yield can be controlled

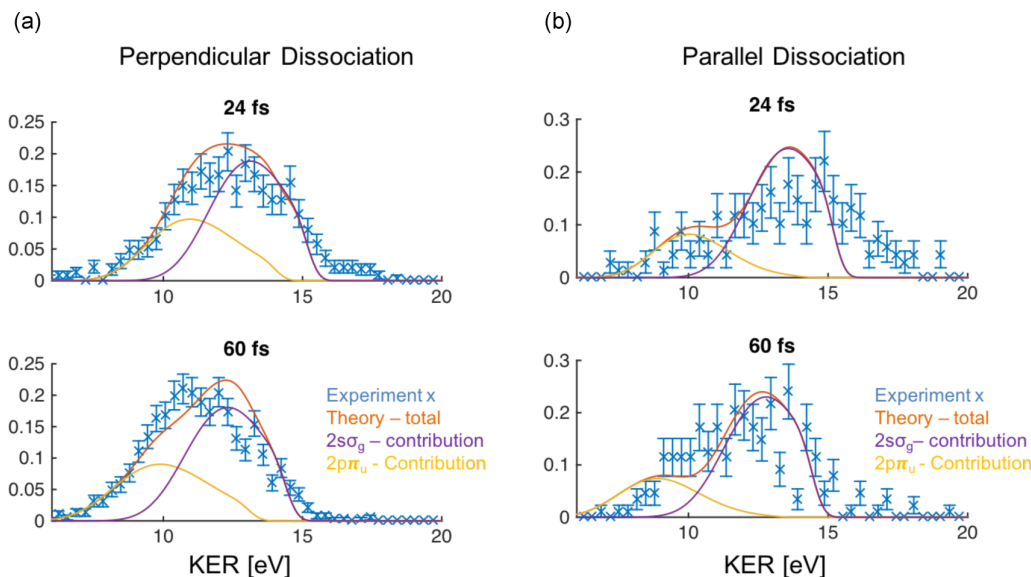


FIG. 3. 1D KER snapshots. (a) Nuclear kinetic energy releases of the Coulomb-exploding molecule at 24 fs and 60 fs delays for the perpendicular dissociation show the snapshots of the dissociative nuclear wave packets at different internuclear distances. Experimental (with error bars) and theoretical data (full orange line). Violet and yellow lines: truncated models including only a single path, through the  $2s\sigma_g$  (violet line) or through the  $2p\pi_u$  (yellow line). The theory shows that the  $2s\sigma_g$  contribution is the largest. (b) Same for the parallel dissociation case, where the  $2s\sigma_g$  is again the dominant channel, although the  $2p\pi_u$  has a smaller relative contribution. In this case, however, the NWP dissociating along the  $2p\pi_u$  potential is doing so at higher velocities compared with the parallel case, separating thus faster from the  $2s\sigma_g$  states. We note here that even at 60 fs delay, there is still an overlap between the two NWPs.

319 by the combined action of the XUV and the IR pulse (for more  
320 details see the Supplemental Material [34]).

321 The molecular orientation with respect to the light po-  
322 larization determines not only the yield of the total double-  
323 ionization signal, as seen in Fig. 2 by comparing the left  
324 and right panels, but also the KER of the fragments obtained  
325 after the Coulomb explosion. These polarization-dependent  
326 features are solely due to the distinct dynamics initiated by  
327 the XUV pump pulse. For each light polarization, a different  
328 nuclear wave packet is created with components [dictated by  
329 the single-ionization amplitudes in Eq. (1)] that evolve along  
330 their corresponding dissociative pathways (see Fig. 1). The  
331 dissociation is mostly governed by the coherent excitation  
332 of the dominant channels: the  $2s\sigma_g$  and  $2p\pi_u$  states. Their  
333 relevance in the interrupted ultrafast dissociative photoioniza-  
334 tion of  $D_2$  can be partly disentangled from the measured  $D^+$   
335 yields. The value of the KER for the bare deuterons observed  
336 at long time delays already discards the contribution of states  
337 correlated with the dissociative channel  $D^+ + D(n=1)$ , as  
338 schematically depicted in Fig. 1 ( $KER = E_1 + E_2$ ). All the  
339 ionic states dissociating into  $D^+ + D(n=2)$  would, however,  
340 lead to similar values of the KER, although, as we will further  
341 show below, by examining the single-ionization step, their  
342 relative weight strongly depends on the molecular orientation.

### 343 III. SIGNATURE OF ELECTRON-ELECTRON 344 CORRELATION IN ULTRAFAST MOLECULAR 345 DISSOCIATION AFTER SINGLE IONIZATION

346 In addition to the time-resolved experiments, we also  
347 performed fully differential synchrotron COLTRIMS exper-

348 iments at a photon energy of 42 eV that reveal the correlated  
349 excitation mechanisms in the molecular-frame photoelectron  
350 angular distributions (MFPADs) upon single ionization. In  
351 Fig. 4(a) we show electron-ion coincidence measurements,  
352 averaged over all electron and deuteron angles, which were  
353 used to identify the states excited by the XUV pulse. These  
354 data are in excellent agreement with those obtained from  
355 near-exact theoretical calculations [Fig. 4(d)] that account  
356 for electron-electron correlation in the initial ground state  
357 as well as in the final states, and during the interaction with  
358 the XUV pulse. The photoelectron energies (electron kinetic  
359 energies, EKE) were measured in coincidence with the kinetic  
360 energy of the  $D^+$  ions (KER) upon dissociative ionization,  
361  $D^+ + D(n)$ . The signals leading to deuterium atoms in a given  
362  $n$  state,  $D(n)$ , follow the energy-conservation lines defined by  
363  $KER + EKE = [h\nu - E_{DIP(n)}]$ , where  $h\nu = 42$  eV and  $E_{DIP(n)}$   
364 is the dissociative ionization potential for the  $D^+ + D(n)$  chan-  
365 nel, namely  $E_{DIP(n=1)} = 18.15$  eV and  $E_{DIP(n=2)} = 28.36$  eV.  
366 These energy-conservation values appear along two diagonal  
367 lines in Figs. 4(a) and 4(d) and correspond to total energies of  
368  $\sim 24$  eV for  $n=1$  and  $\sim 14$  eV for  $n=2$ . The contributions of  
369 the  $1s\sigma_g$  and  $2p\sigma_u$  states are clearly distinguishable along the  
370 coincidence line for  $n=1$ , because a vertical transition from  
371 the ground state to each of them leads to a distinct nuclear  
372 KER, 0–2 eV and 14–21 eV, respectively. The corresponding  
373 signals are weak, which would already explain their minor  
374 contribution in the time-resolved experiment (see Fig. 2).  
375 Moreover, ejection of the second electron from these channels  
376 requires an absorption of a large number of IR photons—  
377 much larger than required for ejecting an electron from highly  
378 excited states (which lie  $\sim 10$  eV closer to the double-ionization



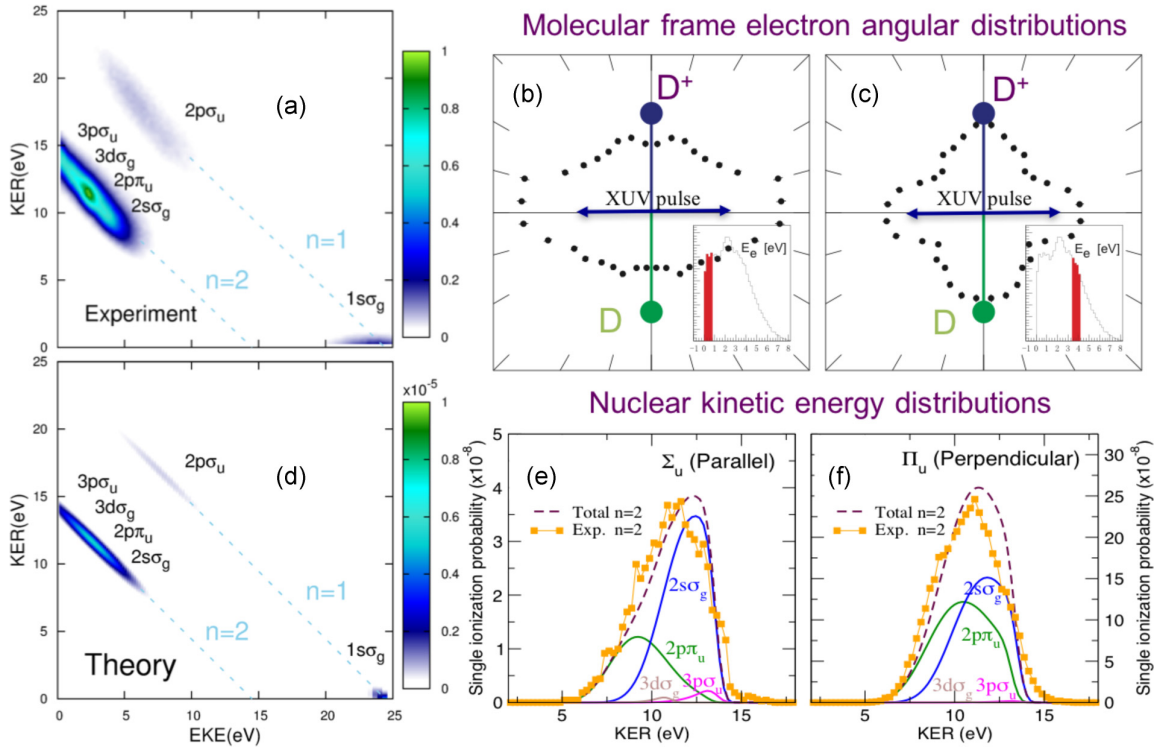


FIG. 4. XUV single ionization probabilities. (a) Nuclear kinetic energy release (KER in  $y$  axis) was measured in coincidence with the photoelectron energy (EKE in  $x$  axis) using COLTRIMS and 42 eV synchrotron radiation to identify all the channels dissociating in the  $D(n=1)$  and  $D(n=2)$  dissociative limit. Contributions from parallel and perpendicular dissociation against the polarization axis are here averaged (see text). Coincidence dashed lines  $NKE + EKE = [42 - E_{DIP(n)}]$  (see text) show maximum available energies of  $\sim 24$  eV and  $\sim 14$  eV for the  $D(n=1)$  and  $D(n=2)$  dissociation limits, respectively. (b) and (c) Experimental MFPADs for two different electron energies and the molecular axis fixed perpendicular to the XUV polarization (as indicated by the purple arrows) show the signature of both  $D_2^+(2s\sigma_g)$  and  $D_2^+(2p\pi_u)$  electronic states. The insets show the two electron energy slices ( $\sim 0.5$  eV and  $\sim 4$  eV) selected from the broad electron kinetic energy distribution in the region of the  $D(n=2)$  limit. (d) Theoretical single ionization probabilities computed for a 7 fs XUV pulse centered at 42.6 eV with an intensity  $I = 10^{12}$  W/cm $^2$ . As in (a), molecules are randomly oriented with respect to the linearly polarized XUV light. (e) and (f) Calculated (thick dashed line) and renormalized experimental (squares) ion yields for the  $D_2^{+*} \rightarrow D^+ + D(n=2)$  dissociation limit for the perpendicular and parallel dissociation directions, integrated over all electron energies. The dominant contributions to the total yield [i.e., dissociative photoionization probabilities for  $n=2$  from (a) and (d) integrated over EKE, in thick dashed line] mostly come from the  $D_2^+(2s\sigma_g)$  (blue) and  $D_2^+(2p\pi_u)$  states (green), with the  $2s\sigma_g$  state being the main excitation channel in *both* orientations. Higher lying states within the  $D(n=2)$  manifold barely contribute and only the  $D_2^+(3p\sigma_u)$  (magenta) and  $D_2^+(3d\sigma_g)$  (brown) are shown in the figure.

379 threshold). Thus, the probability of this process occurring is  
380 very unlikely.

381 The ionization features of the highly excited states  
382 fully overlap along the  $n=2$  coincidence line due to  
383 the repulsive character of all the relevant states in the  
384 Franck-Condon (FC) region and their degeneracy in the  
385 separated-atom limit. All the  $D_2^{+*}$  states corresponding to  
386  $D(n=2)[2s\sigma_g, 3p\sigma_u, 3d\sigma_g, 2p\pi_u, 3d\pi_g, 4f\sigma_u]$  lead to similar  
387 electron kinetic energies, ranging from 0 eV to 6 eV, and  
388 deuteron energies, from 7 eV to 14 eV, which correspond  
389 to the upper and lower limits of the overlap between the  
390 ground-state nuclear wave function and the nuclear wave  
391 functions associated with the highly excited electronic states  
392 in the Franck-Condon region (see Fig. 1). Their relative  
393 population for a particular molecular orientation can be partly  
394 elucidated by examining the electron angular distributions  
395 obtained in the synchrotron radiation experiment [Figs. 4(b)  
396 and 4(c)] and are unambiguously determined from the *ab initio*

397 results for the single-ionization probabilities [Figs. 4(e) and  
398 4(f)]. In Figs. 4(b) and 4(c), we show MFPADs for two electron  
399 energies (0.5 and 3.5 eV) along the electron-ion coincidence  
400 line  $n=2$  for the molecular axis fixed perpendicular to the  
401 XUV light polarization direction. Both MFPADs show a  
402 significant contribution from electrons ejected perpendicular  
403 to the polarization axis. When irradiating a one-active-electron  
404 atomic target, photoionization from an  $s$  state, using linearly  
405 polarized light, leads to a  $p$ -wave dipolar emission pattern  
406 with a node located at right angles with respect to the  
407 polarization axis. In contrast, in a two-active-electron atom  
408 such as He, photoionization above the  $He^+(n=2)$  threshold  
409 (i.e., excitation + ionization with a single photon), which  
410 proceeds through the  $He(2s\epsilon p)$ ,  $He(2p\epsilon s)$ , and  $He(2p\epsilon d)$   
411 channels, may produce a superposition of  $s$ ,  $p$ , and  $d$  waves  
412 (with more complex nodes) whose components depend on the  
413 photoionization branching ratios. For a single-active-electron  
414 molecule (e.g.,  $H_2^+$ ) absorbing linearly polarized light

perpendicular to its molecular axis, the dipole selection rules impose that photoionization from the  $1s\sigma_g$  state can only lead to continuum states of  $\pi_u$  symmetry, hence to MFPADs displaying, as in single-active-electron atoms, a nodal plane perpendicular to the polarization vector. This is why the dominant excitation of the  $2s\sigma_g$  in Fig. 3(a) was surprising. However, for multiple-active-electron molecular targets, even as simple as  $D_2$ , the results of Figs. 4(b) and 4(c) show a significant contribution in the dipole-forbidden region of space. This is caused by the correlation between the ejected photoelectron and the bound electron, which has also been excited by the single XUV photon. Since this bound electron is promoted to a repulsive state of  $D_2^+$ , it acquires a part of the photon energy, but it also acquires part of its angular momentum, while the remaining energy and angular momentum is taken away by the escaping photoelectron [32]. Compared with the time-resolved data [Figs. 2(a), 2(c), and 3(a)], where the excitation probability of the  $2s\sigma_g$  and the  $2p\pi_u$  states is averaged over all the electron energies in the FC region, the MFPADs in Figs. 4(b) and 4(c) provide additional information for the relative ratios of different electronic channels as a function of the electron energy. From Fig. 1, and the correlation energy diagram shown in Fig. 4(a) ( $n = 2$  limit), we see that a low-energy electron is associated with the high-energy  $D^+$  ion in the FC region. Thus, the low-energy-electron MFPAD diagram in Fig. 4(b) can be associated mostly with the upper,  $2s\sigma_g$  state, while the MFPAD associated with the high-energy electron [Fig. 4(c)] should be predominantly coming from the lower,  $2p\pi_u$  state. However, due to the steep potentials in the FC region, it is obvious that both MFPADs have complex angular distributions with different ratios of the  $\sigma_g$  and the  $\pi_u$  angular characteristics. A similar conclusion can be obtained from the MFPADs with ions dissociating parallel to the XUV polarization. As shown in Figs. 2 and 3, the  $2s\sigma_g$  state dominates the dissociation in the parallel direction. Thus, the MFPAD with the most isolated  $2s\sigma_g$  character should be coming from the molecule dissociating along the XUV polarization, and should be associated with the low-energy electron. Figure SM4c (in the Supplemental Material [34]) presents such a case, and, indeed, shows the most isotropic electron angular distribution. For a full data set of MFPAD figures for different molecular-axis orientations see the Supplemental Material [34]. In short, whereas the ground state of  $D_2$  can be described as a configuration interaction of the form  $^1\Sigma_g^+[1s\sigma_g(1)1s\sigma_g(2) + \dots + 2s\sigma_g(1)2s\sigma_g(2) + 2p\pi_u(1)2p\pi_u(2) + \dots]$ , the excitation-ionization states can be described as correlated configurations of the form  $^1\Sigma_u^+[2s\sigma_g(1)\varepsilon s\sigma_u(2) + 2p\pi_u(1)\varepsilon\pi_u(2) + \dots]$  (parallel orientation) and  $^1\Pi_u[2s\sigma_g(1)\varepsilon\pi_u(2) + 2p\pi_u(1)\varepsilon\sigma_g(2) + \dots]$  (perpendicular orientation). Accordingly, while the ionic channels  $D_2^+(2s\sigma_g)$  and  $D_2^+(2p\pi_u)$  clearly participate in both orientations, the MFPADs are determined by the partial waves coming from ejected electrons described by  $\varepsilon\sigma_u$  and  $\varepsilon\pi_g$  states in the parallel case, and  $\varepsilon\pi_u$  and  $\varepsilon\sigma_g$  states in the perpendicular case. Then the MFPADs cannot be simply analyzed with a one-active-electron model. Compared to the previous work done with lower photon energy, where the molecule dissociates in the  $n = 1$  limit [33], these highly differential MFPADs indicate the existence of a strong mixing

between the  $\sigma$  and  $\pi$  states of  $D_2^+$  for both the parallel and perpendicular dissociation cases (see also the molecular frame movies in the Supplemental Material [34] for the complete angular dependence picture).

Finally, in Figs. 4(e) (parallel) and 4(f) (perpendicular orientation), we plot the measured and calculated yields of the  $D^+$  ions upon the XUV excitation process in the asymptotic  $n = 2$  dissociation limit, integrated over the photoelectron energy. Note that the electron-ion coincidence map, shown in Fig. 4(d) for randomly oriented molecules, is obtained with the weighted average of both orientations (1/3 parallel + 2/3 perpendicular). We include the calculated individual contributions from the four lowest electronic states within the  $n = 2$  [ $2s\sigma_g$ ,  $3p\sigma_u$ ,  $2p\pi_u$ , and  $3d\sigma_g$ ] limit, together with the total yields measured in the synchrotron radiation experiment, confirming that the dominant ionization channels correspond to the  $2s\sigma_g$  and  $2p\pi_u$  states. The data in Figs. 4(d) and 4(f) are comparable to the long-delay data shown in Fig. 2, where the dissociation process is finished. Similarly to the time-resolved evolution of the dissociative process, the yields of the  $D^+$  ions in the asymptotic dissociative region, shown in Figs. 4(e) and 4(f), immediately reveal that both parallel and perpendicular excitations involve the  $2s\sigma_g$  and  $2p\pi_u$  states, with  $2s\sigma_g$  being the main excitation channel in both cases. Again, these results cannot be explained by a single-active-electron picture, where only the  $2p\pi_u$  state would be populated in a perpendicular transition from the  $1s\sigma_g$  state. In contrast, for  $n = 1$ , i.e., the ionization case where the outgoing electron does not interact with the second electron, a similar one-active-electron picture predicts that the  $2p\sigma_u$  state should mainly contribute to the parallel transition, which is in agreement with the results of our *ab initio* calculations.

It is worth noting that before this experiment was done, it was not obvious to us that in both directions of the dissociation, the molecule would be excited in a coherent superposition of the  $2s\sigma_g$  and the  $2p\pi_u$  states, with different excitation amplitudes of the two electronic states at hand. In our first try, we manifestly failed to reproduce the experimental data shown in Figs. 2(a) and 2(b) by modeling of the dynamics on an assumption that only the  $2s\sigma_g$   $D_2^+$  state is populated for the parallel orientation, and the  $2p\pi_u$  state is exclusively populated for the perpendicular one. Only by performing nearly exact calculations, that include the electron-electron correlations in the excitation step, we were able to reproduce the data and show that, for both orientations, the molecule is ionized in a coherent superposition of these two states, with different relative weights of the two electronic states. To the best of our knowledge, this complex shake-up process has not been theoretically discussed in the literature and is far from intuitive since the total excitation probability—which dictates the subsequent rapid dissociation—depends strongly on the electron-electron correlation effects, molecular orientation, and the overlap of the  $H_2$  ground state wave function with the steep  $H_2^{+*}$  potentials in the Franck-Condon region.

Once the dominant  $D_2^{+*}$  excitation channels are properly identified, the time-resolved data, shown in Figs. 2 and 3, can be fully understood. First, the relative signal intensity for each molecular orientation is a consequence of the different probabilities for single ionization into the  $D_2^+ 2s\sigma_g$  and  $2p\pi_u$  states. Both of them are much larger for the perpendicular than

for the parallel case [see Figs. 4(e), 4(f)]. Second, the higher asymptotic value of the KER for the parallel case is the result of the larger population of the  $D_2^+ 2s\sigma_g$  state [larger, but not dominant; see Figs. 4(e), 4(f)], which lies higher in energy than the  $D_2^+ 2p\pi_u$  state in the FC region. None of these two features would be observed in the absence of electron-electron correlation either in the  $D_2$  electronic states or during the ionization/excitation process. Ultimately, electron-electron correlation is responsible for changes in the relative population of these states due to changes in the polarization direction of the incoming light, thus leading to a certain degree of control of the  $D^+$  yields under the combined action of the XUV and the IR pulses (see the Supplemental Material [34] for more information).

#### IV. SUMMARY

In conclusion, we have used perfectly synchronized ultrashort high-harmonic XUV and IR pulses, combined with ion 3D momentum imaging detection techniques, to respectively ionize the  $D_2$  molecule and map the dissociation dynamics of a highly excited  $D_2^+$  molecular ion. We have also used synchrotron radiation and electron-ion coincidence imaging to perform highly differential single-ionization measurements to reveal electron correlation effects as seen in the molecular-frame photoelectron angular distributions. Advanced theory shows that the presence of correlations between the two electrons in  $D_2$  dictates the photoexcitation and the resulting dissociation processes. Due to the highly correlated nature of this process, we have found that the mapping of the rapid XUV-induced dissociation dynamics shows up in the form of a coherent superposition of several electronic states. The

quantitative analysis of the correlation effects in this highly excited region of  $H_2^+$  would be important for future attosecond XUV/XUV pump/probe experiments that would allow for measuring of the molecular-frame temporal coherences, as seen in Fig. 2(c). Also, we envision that the use of single-attosecond XUV pulses would allow for perfect control over the localization of the electron wave function in the  $n = 2$  dissociative limit.

#### ACKNOWLEDGMENTS

The authors gratefully acknowledge support from the DOE Office of Basic Energy Sciences (AMOS program, DE-FG02-99ER14982), the Advanced Grant of the ERC XCHEM 290853, the European COST Action XLIC CM1204, and the MINECO Project No. FIS2013-42002-R. J.L.S.V. was supported by Vicerrectoría de Investigación (Project No. E01538 and Estrategia de Sostenibilidad) at Universidad de Antioquia and COLCIENCIAS under Grant No. 111565842968. X.M.T. was supported by a Grand-in-Aid for Scientific Research from the Japan Society for the Promotion of Science. This research used the Advance Light Source and resources of the National Energy Research Scientific Computing Center, DOE Office of Science User Facilities supported by the Director, Office of Science, Office of Basic Energy Sciences, the Division of Chemical Sciences, Geosciences, and Biosciences of the US Department of Energy at LBNL under Contract No. DE-AC02-05CH11231. We acknowledge funding by the Deutsche Forschungsgemeinschaft and DAAD. We thank the staff of the Advanced Light Source, in particular beamline 9.3.2 scientist B. S. Mun for his outstanding support. P.R. thanks RoentDek for their continuous support with the COLTRIMS software and hardware.

- [1] D. Akoury, K. Kreidi, T. Jahnke, T. Weber, A. Staudte, M. Schoeffler, N. Neumann, J. Titze, L. P. H. Schmidt, A. Czasch, O. Jagutzki, R. A. C. Fraga, R. E. Grisenti, R. Diez Muino, N. A. Cherepkov, S. K. Semenov, P. Ranitovic, C. L. Cocke, T. Osipov, H. Adaniya, J. C. Thompson, M. H. Prior, A. Belkacem, A. L. Landers, H. Schmidt-Boecking, and R. Doerner, *Science* **318**, 949 (2007).
- [2] A. Alnaser, B. Ulrich, X. Tong, I. Litvinyuk, C. Maharjan, P. Ranitovic, T. Osipov, R. Ali, S. Ghimire, Z. Chang, C. Lin, and C. Cocke, *Phys. Rev. A* **72**, 030702 (2005).
- [3] T. Ergler, B. Feuerstein, A. Rudenko, K. Zrost, C. D. Schroter, R. Moshhammer, and J. Ullrich, *Phys. Rev. Lett.* **97**, 103004 (2006).
- [4] G. D. Dickenson, M. L. Niu, E. J. Salumbides, J. Komasa, K. S. E. Eikema, K. Pachucki, and W. Ubachs, *Nature* **410**, 193601 (2013).
- [5] M. Drescher, M. Hentschel, R. Kienberger, M. Uiberacker, V. Yakovlev, A. Scrinzi, T. Westerwalbesloh, U. Kleineberg, U. Heinzmann, and F. Krausz, *Nature (London)* **419**, 803 (2002).
- [6] A. L. Cavalieri, N. Mueller, T. Uphues, V. S. Yakovlev, A. Baltuska, B. Horvath, B. Schmidt, L. Bluemel, R. Holzwarth, S. Hendel, M. Drescher, U. Kleineberg, P. M. Echenique, R. Kienberger, F. Krausz, and U. Heinzmann, *Nature (London)* **449**, 1029 (2007).
- [7] L. Miaja-Avila, G. Saathoff, S. Mathias, J. Yin, C. La-o-Vorakiat, M. Bauer, M. Aeschlimann, M. M. Murnane, and H. C. Kapteyn, *Phys. Rev. Lett.* **101**, 046101 (2008).
- [8] E. Gagnon, P. Ranitovic, X.-M. Tong, C. L. Cocke, M. M. Murnane, H. C. Kapteyn, and A. S. Sandhu, *Science* **317**, 1374 (2007).
- [9] M. Schultze, M. Fiess, N. Karpowicz, J. Gagnon, M. Korbman, M. Hofstetter, S. Neppl, A. L. Cavalieri, Y. Komninos, T. Mercouris, C. A. Nicolaides, R. Pazourek, S. Nagele, J. Feist, J. Burgdoerfer, A. M. Azzeer, R. Ernstorfer, R. Kienberger, U. Kleineberg, E. Goulielmakis, F. Krausz, and V. S. Yakovlev, *Science* **328**, 1658 (2010).
- [10] P. Johnsson, J. Mauritsson, T. Remetter, A. L'Huillier, and K. J. Schafer, *Phys. Rev. Lett.* **99**, 233001 (2007).
- [11] P. Ranitovic, X. M. Tong, C. W. Hogle, X. Zhou, Y. Liu, N. Tushima, M. M. Murnane, and H. C. Kapteyn, *Phys. Rev. Lett.* **106**, 193008 (2011).
- [12] E. Turgut, C. La-O-Vorakiat, J. M. Shaw, P. Grychtol, H. T. Nembach, D. Rudolf, R. Adam, M. Aeschlimann, C. M. Schneider, T. J. Silva, M. M. Murnane, H. C. Kapteyn, and S. Mathias, *Phys. Rev. Lett.* **110**, 197201 (2013).
- [13] E. Goulielmakis, Z.-H. Loh, A. Wirth, R. Santra, N. Rohringer, V. S. Yakovlev, S. Zherebtsov, T. Pfeifer, A. M. Azzeer, M. F.

- Kling, S. R. Leone, and F. Krausz, *Nature (London)* **466**, 739 (2010).
- [14] H. Wang, M. Chini, S. Chen, C.-H. Zhang, F. He, Y. Cheng, Y. Wu, U. Thumm, and Z. Chang, *105*, 143002 (2010). **11**
- [15] H. J. Worner, H. Niikura, J. B. Bertrand, P. B. Corkum, and D. M. Villeneuve, *Phys. Rev. Lett.* **102**, 103901 (2009). **12**
- [16] E. Skantzakis, P. Tzallas, J. E. Kruse, C. Kalpouzos, O. Faucher, G. D. Tsakiris, and D. Charalambidis, *105*, 043902 (2010). **13**
- [17] M. Holler, F. Schapper, L. Gallmann, and U. Keller, *106*, 123601 (2011). **14**
- [18] F. Calegari, D. Ayuso, A. Trabattoni, L. Belshaw, S. De Camillis, S. Anumula, F. Frassetto, L. Poletto, A. Palacios, P. Decleva, J. B. Greenwood, F. Martin, and M. Nisoli, *Science* **346**, 336 (2014).
- [19] F. Kelkensberg, W. Siu, J. F. Perez-Torres, F. Morales, G. Gademann, A. Rouzee, P. Johnsson, M. Lucchini, F. Calegari, J. L. Sanz-Vicario, F. Martin, and M. J. J. Vrakking, *107*, 043002 (2011). **15**
- [20] K. P. Singh, F. He, P. Ranitovic, W. Cao, S. De, D. Ray, S. Chen, U. Thumm, A. Becker, M. M. Murnane, H. C. Kapteyn, I. V. Litvinyuk, and C. L. Cocke, *104*, 023001 (2010). **16**
- [21] G. Sansone, F. Kelkensberg, J. F. Perez-Torres, F. Morales, M. F. Kling, W. Siu, O. Ghafur, P. Johnsson, M. Swoboda, E. Benedetti, F. Ferrari, F. Lepine, J. L. Sanz-Vicario, S. Zharebtsov, I. Znakovskaya, A. L'Huillier, M. Y. Ivanov, M. Nisoli, F. Martin, and M. J. J. Vrakking, *Nature (London)* **465**, 763 (2010).
- [22] Y. Furukawa, Y. Nabekawa, T. Okino, S. Saugout, K. Yamanouchi, and K. Midorikawa, *Phys. Rev. A* **82**, 013421 (2010).
- [23] A. Fischer, A. Sperl, P. Cörlin, M. Schönwald, H. Rietz, A. Palacios, A. González-Castrillo, F. Martín, T. Pfeifer, J. Ullrich, A. Senftleben, and R. Moshhammer, *110*, 213002 (2013). **17**
- [24] P. Ranitovic, C. W. Hogle, P. Rivière, A. Palacios, X.-M. Tong, N. Tushima, A. González-Castrillo, L. Martin, F. Martín, and M. M. Murnane, *Proc. Natl. Acad. Sci. USA* **111**, 912 (2014).
- [25] M. Ossiander, F. Siegrist, V. Shirvanyan, R. Pazourek, A. Sommer, T. Latka, A. Guggenmos, S. Nagele, J. Feist, J. Burgdörfer, R. Kienberger, and M. Schultze, *Nat. Phys.* **13**, 280 (2016).
- [26] L. Cattaneo, J. Vos, R. Y. Bello, A. Palacios, S. Heuser, L. Pedrelli, M. Lucchini, C. Cirelli, F. Martin, and U. Keller, *Nat. Phys.*, doi: (2018). **18**
- [27] M. Waitz, R. Y. Bello, D. Metz, J. Lower, F. Trinter, C. Schober, M. Keiling, U. Lenz, M. Pitzer, K. Mertens, M. Martins, J. Viefhaus, S. Klumpp, T. Weber, L. P. H. Schmidt, J. B. Williams, M. S. Schöffler, V. V. Serov, A. S. Kheifets, L. Argenti, A. Palacios, F. Martin, T. Jahnke, and R. Dörner, *Nat. Commun.* **8**, 2266 (2017).
- [28] E. Gagnon, A. S. Sandhu, A. Paul, K. Hagen, A. Czasch, T. Jahnke, P. Ranitovic, C. Lewis Cocke, B. Walker, M. M. Murnane, and H. C. Kapteyn, *Rev. Sci. Instrum.* **79**, 063102 (2008).
- [29] A. Rundquist, C. Durfee, Z. Chang, C. Herne, S. Backus, M. Murnane, and H. Kapteyn, *Science* **280**, 1412 (1998).
- [30] S. Backus, C. G. Durfee III, M. M. Murnane, and H. C. Kapteyn, *Rev. Sci. Instrum.* **69**, 1207 (1998).
- [31] R. Dörner, V. Mergela, O. Jagutzkia, L. Spielbergera, J. Ullrichb, R. Moshhammerb, and H. Schmidt-Böckinga, *Phys. Rep.* **330**, 95 (2000).
- [32] T. Jahnke, J. Titze, L. Foucar, R. Wallauer, T. Osipov, E. P. Benis, O. Jagutzki, W. Arnold, A. Czasch, A. Staudte, M. Schöffler, A. Alnaser, T. Weber, M. H. Prior, H. Schmidt-Bocking, and R. Dörner, *183*, 48 (2011). **19**
- [33] A. Lafosse, M. Lebech, J. C. Brenot, P. M. Guyon, L. Spielberger, O. Jagutzki, J. C. Houver, and D. Dowek, *J. Phys. B: At., Mol. Opt. Phys.* **36**, 4683 (2003).
- [34] See Supplemental Material at <http://link.aps.org/supplemental/10.1103/PhysRevA.00.002500> for more information. **20**